Environmental Pollution 269 (2021) 116167

Contents lists available at ScienceDirect

Environmental Pollution

journal homepage: www.elsevier.com/locate/envpol

Model vs. observation discrepancy in aerosol characteristics during a half-year long campaign in Northeast China: The role of biomass burning

Yuan Cheng [a], Qin-qin Yu [a], Jiu-meng Liu [a, *], Shengqiang Zhu [b], Mengyuan Zhang [b], Hongliang Zhang [b], Bo Zheng [c], Ke-bin He [d]

[a] State Key Laboratory of Urban Water Resource and Environment, School of Environment, Harbin Institute of Technology, Harbin, China
[b] Department of Environmental Science and Engineering, Fudan University, Shanghai, China
[c] Laboratoire des Sciences Du Climat et de L'Environnement, CEA-CNRS-UVSQ, UMR8212, Gif-sur-Yvette, France
[d] State Key Joint Laboratory of Environment Simulation and Pollution Control, School of Environment, Tsinghua University, Beijing, China

ARTICLE INFO

Article history:
Received 24 September 2020
Received in revised form
24 November 2020
Accepted 25 November 2020
Available online 26 November 2020

Keywords:
Agricultural fires
CMAQ
Organic aerosol
Elemental carbon
Secondary inorganic aerosol

ABSTRACT

Complex air pollutant sources and distinct meteorological conditions resulted in unique wintertime haze pollution in the Harbin-Changchun (HC) metropolitan area, China's only national-level city cluster located in the severe cold climate region. In this study, field observation and air quality modeling were combined to investigate fine particulate matter ($PM_{2.5}$) pollution during a six-month long heating season in HC's central city (Harbin). The model significantly underpredicted $PM_{2.5}$ and organic carbon (by up to ~230 $\mu g/m^3$ and 110 $\mu gC/m^3$, respectively, in terms of daily average) when levoglucosan concentrations were above 0.5 $\mu g/m^3$. Based on a synthesis of levoglucosan concentrations and fire counts, the large gaps were attributed to underestimation of open burning emissions by the model. However, the model tended to overpredict elemental carbon (more significantly at higher NO_2), likely pointing to an overestimation of vehicle emissions. With increasing levoglucosan, the difference between observed and simulated nitrate ($nitrate_{obs}$ – $nitrate_{mod}$, i.e., Δnitrate) showed a transition from negative to positive values. The positive Δnitrate were attributed to underprediction of the open-burning related nitrate, whereas the negative Δnitrate were likely caused by overprediction of nitrate from other sources (presumably vehicle emissions). The dependence of Δnitrate on levoglucosan indicated that with stronger impact of open burning, the overprediction effect was gradually offset and finally overwhelmed. Influence of open burning on sulfate formation was evident as well, but less apparent compared to nitrate. This study illustrates how the uncertainties in open burning emissions will influence $PM_{2.5}$ simulation, on not only primary components but also secondary species.

1. Introduction

Stringent clean air actions have been conducted to address the severe haze pollution in China, under the "Air Pollution Prevention and Control Action Plan" and the "Three-Year Action Plan for Winning the Blue Sky Defense Battle" promulgated by the State Council of China in 2013 and 2018, respectively. With the implementation of these actions, considerable changes were identified for ozone (O_3) and particles with aerodynamic diameters ≤ 2.5 μm ($PM_{2.5}$), e.g., O_3 tended to increase in some regions of China despite a nationwide decrease of $PM_{2.5}$ concentration (Li et al., 2019b; Wei et al., 2019; Zhai et al., 2019; Zhang et al., 2019). The control measures influenced chemical composition of $PM_{2.5}$ as well. For example, aerosol mass spectrometer (AMS) measurements performed during winter in Beijing pointed to an increasing trend for the nitrate-to-sulfate ratio in recent years (Li et al., 2019a; Xu et al., 2019; Gu et al., 2020), and this trend was suggested to be primarily associated with the more rapid decrease of sulfur dioxide (SO_2) emissions compared to nitrogen oxides (NO_x). The AMS-based studies also indicated changes in organic aerosol (OA) composition. A noticeable feature was that the contribution of biomass

This paper has been recommended for acceptance by Admir C. Targino.
* Corresponding author.
E-mail addresses: ycheng@hit.edu.cn (Y. Cheng), jiumengliu@hit.edu.cn (J.-m. Liu).

https://doi.org/10.1016/j.envpol.2020.116167
0269-7491/

burning OA almost doubled since the winter of 2014–2015 (~20%; Li et al., 2019a) compared to the previous ones (~10% for the winter of 2010–2011 through that of 2013–2014; Hu et al., 2016b; Sun et al., 2016a and 2018), which was likely caused by a substantial reduction of coal combustion emissions (Xu et al., 2019). Therefore, comprehensive information on $PM_{2.5}$, especially its chemical composition, is essential for the evaluation of various air pollution control measures.

In addition to field observations, chemically-resolved $PM_{2.5}$ concentrations could also be derived from chemical transport models such as Community Multi-scale Air Quality (CMAQ). However, discrepancies usually exist between observed and simulated $PM_{2.5}$ components, resulting in challendges for understanding of $PM_{2.5}$ sources and formation mechanisms, and consequently the design of $PM_{2.5}$ control policies. For example, Liu et al. (2020) found that the abundances and temporal variations of OA measured during winter in Beijing could not be properly reproduced by CMAQ, with the observed organic carbon (OC) to elemental carbon (EC) ratios being ~100% higher than modeling results under high relative humidity (RH) conditions. At high RH, sulfate was also significantly underestimated during winter in Beijing using either CMAQ (Zheng et al., 2015) or the Goddard Earth Observing System with chemistry (GEOS-Chem), another commonly-used model (Wang et al., 2014). The high-RH related discrepancies were thought to be caused primarily by the missing of heterogeneous chemistry in models, especially the missing of reactions occurring in aerosol water (e.g., Cheng et al., 2016). These findings give rise to a new concept termed "haze chemistry" (Chu et al., 2020), of which an important feature was the RH-dependent enhancement of secondary species during winter haze events. In addition to the components influenced by secondary formation, the model vs. observation difference could also be evident for primary aerosols such as black carbon (BC, referred broadly to results from various measurement principles, e.g., EC determined from thermal-optical method). For example, during Phase II of the AeroCom model intercomparison project, an overprediction of BC concentration was found for remote ocean regions, which was attributed to the overlong BC lifetime assumed by the models (Samset et al., 2014). Therefore, to bridge the gaps between observational and modeling results of $PM_{2.5}$, continuous efforts are needed for a better understanding of each step along the way from emission to fate of both primary aerosol and precursors of secondary aerosol.

Historically, studies on $PM_{2.5}$, either measurement- or model-based, have been most frequently conducted at a limited number of air pollution hotpots in China, e.g., the North China Plain (NCP; e.g., Cai et al., 2017; Dao et al., 2019) and the Yangtze River Delta (e.g., Cheng et al., 2014; Ming et al., 2017). Correspondingly, other regions with different characteristics of air pollutant emissions and/or meteorological conditions are largely overlooked, prohibiting a more comprehensive understanding of the diversity of haze pollution in Chinese cities. The Harbin-Changchun (HC) metropolitan area, which is located in the severe cold climate region in Northeast China, is such a "forgotten" city cluster. Despite the increasing attention on severe haze pollution in HC, no significant reduction in $PM_{2.5}$ levels has been achieved for the heating season (mid-October to mid-April of next year) in recent years. For example, the peak values of monthly average $PM_{2.5}$ stayed above 100 $\mu g/m^3$ during the past seven heating seasons in Harbin (HC's central city), as can be seen from the air quality data routinely published on China's National Urban Air Quality Real Time Publishing Platform (http://106.37.208.233:20035/). The HC region differs with other regions in China from the following aspects. The first one is the extremely cold winter when the daily average temperature could be as low as below −20 °C. Second reason is the complex air pollutant sources during heating season, with agricultural fire emissions overlaying on top of other anthropogenic sources like coal combustion and vehicle emissions (Cheng et al., 2021). Particularly, it has been recognized that there exist substantial uncertainties in the detection of agricultural fires as well as the estimation of their emissions and impacts (Qiu et al., 2016; Zhou et al., 2017; Uranishi et al., 2019; Wang et al., 2020). For example, $PM_{2.5}$ emissions from open burning in Northeast China were shown to differ by approximately one order of magnitude among various inventories (Uranishi et al., 2019). In addition, little is known about the atmospheric chemistry processes in this unique frigid environment with emissions from various sources. Obviously, such information could not be obtained from studies in other regions of China.

In this study, field observation and air quality modeling were integrated to investigate the characteristics of $PM_{2.5}$ pollution during a six-month long heating season in HC. To our knowledge, this study is the first of this kind for HC. Our analyses showed large discrepancies between model and observation results not only on $PM_{2.5}$ mass concentration but also on its chemical composition, and uncovered that the discrepancies are strongly associated with open burning. Compared to results retrieved from other regions of China such as Beijing, this study provided additional implications for the improvement of air quality models.

2. Methods

2.1. Field observation

A measurement campaign was conducted during the 2018–2019 heating season at an urban site in Harbin, as described in Cheng et al. (2020, 2021). Briefly, a total of 180 $PM_{2.5}$ samples (24-h integrated) were collected on the campus of Harbin Institute of Technology (45°45′24″ N, 126°40′49″ E) from October 16, 2018 to April 14, 2019. The sampling was performed by a low volume sampler (MiniVol; Airmetrics, OR, USA), which was operated with pre-baked quartz-fiber filters (2500 QAT-UP; Pall Corporation, NY, USA) at a flow rate of 5 L/min. The samples were analyzed for OC and EC using a DRI Thermal/Optical Carbon Analyzer (Model 2001; Atmoslytic Inc., CA, USA), by the IMPROVE-A temperature protocol with transmittance charring correction. In addition, water-soluble inorganic ions such as sulfate (SO_4^{2-}), nitrate (NO_3^-) and ammonium (NH_4^+) were determined using a Dionex ion chromatography (IC) system (ICS-5000$^+$; Thermo Fisher Scientific Inc., MA, USA). The IC was also used to measure levoglucosan by the high-performance anion-exchange chromatography coupled to pulsed amperometric detection (HPAEC-PAD) method. Two samples showed concentrations below LOD (limits of detection) and were excluded in the following analyses. Based on the quantified species, observation-based $PM_{2.5}$ concentration was constructed as the sum of OA (determined as 1.6 × OC), EC and the inorganic ions. Consistency between the constructed and measured $PM_{2.5}$ concentrations as well as ion balance between the cations and anions were demonstrated in Cheng et al. (2020).

2.2. Air quality modeling

The mass concentration and chemical composition of $PM_{2.5}$ were simulated for the measurement period using a revised CMAQ model (Hu et al., 2016a). Compared to the original version (5.0.1), the revised model involved a modified Statewide Air Pollution Research Center (version 11; SAPRC-11) photochemical mechanism, which includes the isoprene epoxydiols (IEPOX) and methacrylic acid epoxide formation pathways, and allows predictions of glyoxal and methylglyoxal formed by oxidation of various precursors

including isoprene. In addition, heterogeneous pathways were incorporated into the revised CMAQ to account for secondary inorganic and organic aerosols formed through reactive uptake of gaseous species on aerosol surfaces. In this study, the simulations were performed over East Asia with a horizontal resolution of 36 × 36 km. The meteorological inputs were retrieved from the Weather Research and Forecasting (WRF) model. The emission inputs were generated by combining various inventories, e.g., the Multi-resolution Emission Inventory for China (MEIC; http://www.meicmodel.org/) was used to derive anthropogenic emissions of OC, EC, volatile organic compounds (VOCs), SO_2, NO_2, etc., whereas the satellite-based Fire INventory from NCAR (FINN; Wiedinmyer et al., 2011) was used for open burning emissions. To compare with the observational data, modeling results were extracted for the grid cell where the sampling site is located. Refer to the Supplementary material for model performance.

3. Results and discussion

3.1. Open-burning related underprediction of $PM_{2.5}$

Fig. 1a compares the observed and modeled $PM_{2.5}$ concentrations ($PM_{2.5obs}$ and $PM_{2.5mod}$, respectively) for the entire heating season. $PM_{2.5mod}$ was significantly lower than $PM_{2.5obs}$ for a considerable fraction of samples, e.g., by as much as ~230 μg/m^3 for the sample collected from February 26 to 27, 2019. This sample was characterized by the highest levoglucosan concentration during the campaign (14.56 μg/m^3), and the corresponding levoglucosan-to-OC ratio (LG/OC) was as high as ~5% (on a basis of carbon mass). In addition, this sample was collected during the relatively warm segment of this study, when the daily average temperatures were ~0 °C, indicating that the high levoglucosan concentration observed for this sample should not be caused by household use of biomass (e.g., for heating). Actually, the occurrences of high levoglucosan concentration and high LG/OC ratio were irregular during the measurement period, and no dependence of either levoglucosan or LG/OC on temperature was observed (Figure S1). Thus it was inferred that the temporal variation of levoglucosan was mainly driven by open burning rather than residential combustion of biomass fuels. This inference was also supported by the fire count results. For example, as shown in Fig. 2, intensive open burning was

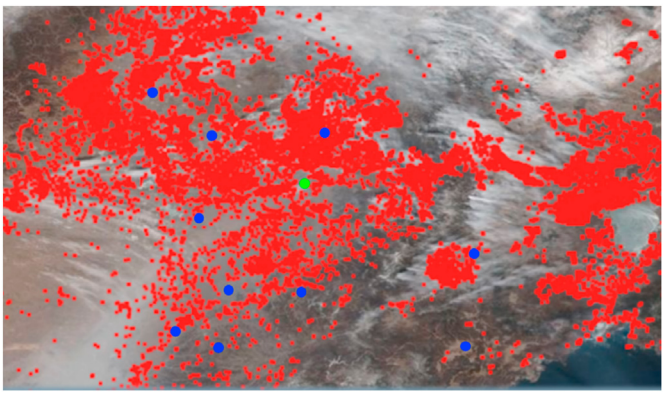

Fig. 2. The Visible Infrared Imaging Radiometer Suite (VIIRS) true-color image around the HC metropolitan area during February 25 to March 2, 2019, overlaid with the active fire detections as red dots. The image was created using the Fire Information for Resource Management System (FIRMS; https://firms.modaps.eosdis.nasa.gov/). Cities in HC are highlighted by the solid circles, with Harbin in green and others in blue. (For interpretation of the references to color in this figure legend, the reader is referred to the Web version of this article.)

evident for a 6-day period (from February 25 to March 2, 2019) showing continuously high levoglucosan concentrations (4.10–14.56 μg/m^3). Given that elevated levoglucosan prevailed from December throughout mid-April (Figure S1), it appears that the open burning activities in HC and its surrounding areas were not concentrated within a specific (or short-term) period. This is different from other regions in China. For example, in NCP, open burning episodes caused by post-harvest combustion of wheat straw, which typically lasted for only 1–2 weeks, were repeatedly observed during late June in recent years (Cheng et al., 2013; Sun et al., 2016b, 2018; Yan et al., 2019). This difference could be mainly attributed to the regional variation of agricultural production activities. The double-cropping system (usually wheat-maize system) in NCP requires the crop residues disposed within a relatively short period. But in the HC region, due to the extremely cold winter, crops such as corn and wheat are usually planted in late spring and harvested in early autumn. This leads to a relatively long period, which largely overlaps with the heating season, for the

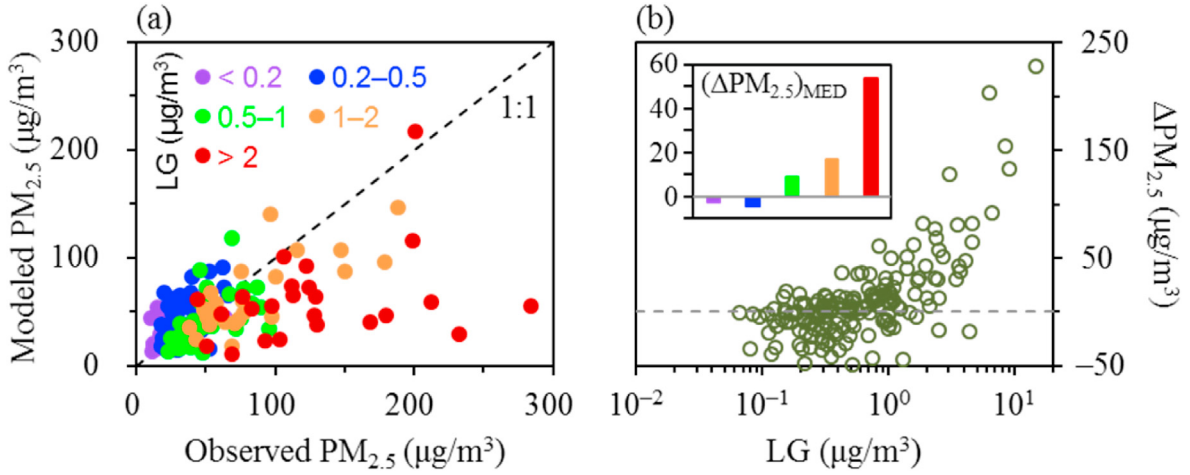

Fig. 1. **(a)** Comparison of observed and modeled $PM_{2.5}$ concentrations. Results from different levoglucosan (LG) ranges are shown using various markers. The dashed line indicates a one-to-one correspondence. **(b)** Dependence of the difference between observed and modeled $PM_{2.5}$ concentrations ($PM_{2.5obs}$ – $PM_{2.5mod}$, i.e., $\Delta PM_{2.5}$) on levoglucosan. The dashed line indicates a $\Delta PM_{2.5}$ value of zero. The inner bar chart in (b) shows the median $\Delta PM_{2.5}$ values (in μg/m^3), i.e., $(\Delta PM_{2.5})_{MED}$, in five successive bins with levoglucosan concentrations of below 0.2 (purple), 0.2–0.5 (blue), 0.5–1 (green), 1–2 (orange) and above 2 μg/m^3 (red), respectively. (For interpretation of the references to color in this figure legend, the reader is referred to the Web version of this article.)

disposal of crop residues. According to the agricultural fire bans released by the government of Heilongjiang province (where Harbin is located at) in 2018, open burning was strictly prohibited in its whole domain area from September 15 to December 10 of 2018, and from March 10 to May 15 of 2019 (Department of Ecology and Environment of Heilongjiang Province, 2018). For the 2018–2019 heating season, therefore, there was a wide window of approximately 3 months left for the disposal of crop residues. Interestingly, although the agricultural fires spanned for 3–4 months in HC (as suggested by Figure S1), the levoglucosan concentrations and LG/OC ratios were frequently higher than those from the concentrated open burning episodes encountered during late June in NCP. For example, during such an episode in Beijing, the average levoglucosan concentration and LG/OC ratio were 0.75 μg/m^3 and 1.5%, respectively (Cheng et al., 2013), lower than the respective values for the entire measurement period of this study (1.06 μg/m^3 and 1.8%). Given that the spatial variation of LG/OC was not influenced by meteorological conditions (e.g., wind speed and planetary boundary layer height), the influence of open burning, i.e., agricultural fires, was persistent and strong in HC.

The comparison of $PM_{2.5obs}$ and $PM_{2.5mod}$ was shown in Fig. 1a, color-coded by different levoglucosan abundances. The revised CMAQ was found to underpredict $PM_{2.5}$ more significantly with increasing levoglucosan, i.e., with stronger impact of open burning. This pattern was more directly reflected in Fig. 1b, as can be seen from the larger difference between the observed and modeled $PM_{2.5}$ ($\Delta PM_{2.5}$, which equals to $PM_{2.5obs} - PM_{2.5mod}$) at higher levoglucosan. Fig. 1b also compares $\Delta PM_{2.5}$ across different levoglucosan ranges (refer to Figure S2a for the detailed box plot). The median $\Delta PM_{2.5}$ was essentially close to zero for the first two bins with levoglucosan below 0.5 μg/m^3, increased to ~9 μg/m^3 for the levoglucosan range of 0.5–1 μg/m^3, further increased to ~17 μg/m^3 when levoglucosan were between 1 and 2 μg/m^3, and final reached ~54 μg/m^3 for the last bin with levoglucosan above 2 μg/m^3. Both Fig. 1a and b indicated that the modeled $PM_{2.5}$ concentrations were substantially lower than the observational results when heavily impacted by agricultural fires, e.g., $\Delta PM_{2.5}$ stayed above 90 μg/m^3 at the extremely high levoglucosan concentrations of above 5 μg/m^3, and the corresponding $\Delta PM_{2.5}/PM_{2.5obs}$ were as high as ~70–90%.

The levoglucosan-dependent underprediction of $PM_{2.5}$ pointed to underestimation of open burning emissions, which were obtained from the FINN inventory in the revised CMAQ. The same conclusion was reached by Uranishi et al. (2019), which suggested that for Northeast China, the FINN-based agricultural fire emissions needed to be increased by 20 times to explain the observed $PM_{2.5}$ concentrations in the fall of 2014. Other inventories relying on the satellite remote sensing of burned area, e.g., the Global Fire Emissions Database (GFED), appear to underestimate open burning emissions as well (Reddington et al., 2016, 2019; Lasko et al., 2017; Konovalov et al., 2018; Pan et al., 2020). The underestimation can be caused by many region-dependent factors such as missing of small-scale and understory fires, missing of fires due to satellite overpass timing and cloud cover, etc. Regarding field observations, although it is generally practical to identify apparent open burning episodes, it is difficult to robustly distinguish the emissions from open burning with that associated with household combustion of biofuels. In this study, given that a sharp increase of $\Delta PM_{2.5}$ could not be identified unless levoglucosan exceeded 0.5 μg/m^3, a levoglucosan concentration of above 0.5 μg/m^3 was considered as the indicator for evident influence of open burning.

3.2. Open-burning related underprediction of OC

Observational results showed that the particle mass was generally dominated by organic aerosol during the measurement period, with an average OA-to-$PM_{2.5}$ ratio of 0.59 ± 0.07. However, the dominant contribution of OA could not be reproduced by the model, as indicated by the substantially lower OA-to-$PM_{2.5}$ ratios derived from the revised CMAQ (averaging 0.40 ± 0.11). In addition, similar to the comparison for $PM_{2.5}$ concentration, the model also underpredicted the organic mass for a substantial fraction of samples (Fig. 3a), and the difference between observed and modeled OC ($OC_{obs} - OC_{mod}$, i.e., ΔOC) depended positively on levoglucosan as well (Fig. 3b). Fig. 3b also compares ΔOC across different levoglucosan ranges (refer to Figure S2b for the detailed box plot). OC_{mod} and OC_{obs} were found to be generally comparable for the two bins with levoglucosan below 0.5 μg/m^3, showing median ΔOC concentrations of ~2.5 μgC/m^3. However, ΔOC were substantially larger at higher levoglucosan, with median values of ~8.5, 11 and 28 μgC/m^3 for the levoglucosan ranges of 0.5–1, 1–2 and above 2 μg/m^3, respectively. At the extremely high levoglucosan concentrations of above 5 μg/m^3, ΔOC reached ~45–110 μgC/m^3

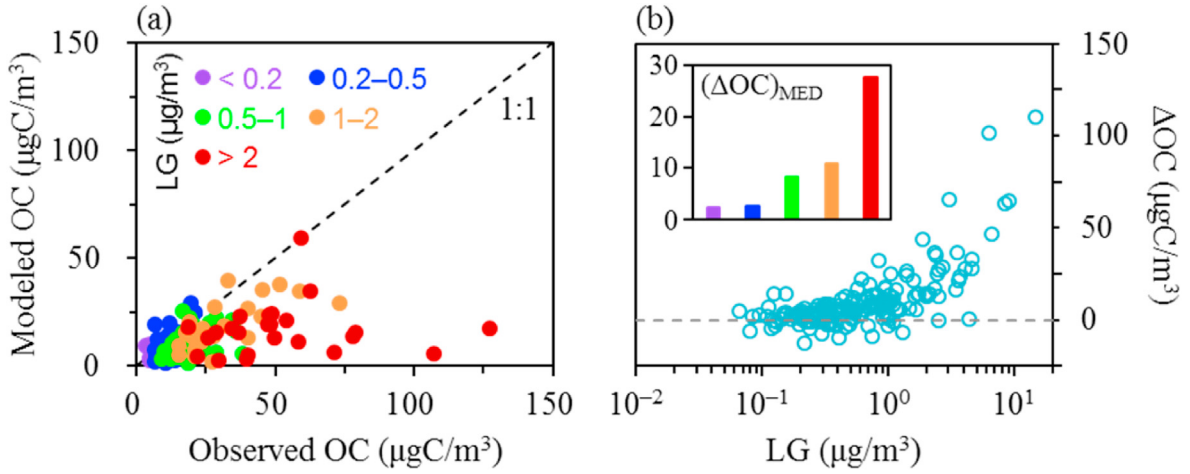

Fig. 3. **(a)** Comparison of observed and modeled OC concentrations. Results from different levoglucosan ranges are shown with various markers. The dashed line indicates a one-to-one correspondence. **(b)** Dependence of the difference between observed and modeled OC concentrations ($OC_{obs} - OC_{mod}$, i.e., ΔOC) on levoglucosan. The dashed line indicates a ΔOC value of zero. The inner bar chart in (b) shows the median ΔOC values (in μgC/m^3), i.e., $(\Delta OC)_{MED}$, in five successive bins with levoglucosan concentrations of below 0.2 (purple), 0.2–0.5 (blue), 0.5–1 (green), 1–2 (orange) and above 2 μg/m^3 (red), respectively. (For interpretation of the references to color in this figure legend, the reader is referred to the Web version of this article.)

and accounted for 80–95% of OC_{obs}, pointing to a dramatic underestimation of organic aerosol by the revised CMAQ when the open burning impacts are significant.

The majority of the samples with evident influence of open burning, i.e., with levoglucosan above 0.5 μg/m^3, showed positive values for both ΔOC and $\Delta PM_{2.5}$. For these samples, ΔOC exhibited a strong positive dependence on $\Delta PM_{2.5}$ (Figure S3), with a slope of 0.49 ± 0.01 (intercept was set as zero; $R^2 = 0.94$). This slope could be translated to a ΔOA to $\Delta PM_{2.5}$ contribution of 78%, suggesting that the underestimation of $PM_{2.5}$ mass by the revised CMAQ was mainly caused by the underprediction of OA (or OC). The high ΔOA to $\Delta PM_{2.5}$ contribution derived in this case, mainly associated with open burning, was consistent with previous results from biomass burning source emission studies. For example, emissions from agricultural fires in the southeastern U.S. were measured during the Studies of Emissions and Atmospheric Composition, Clouds and Climate Coupling by Regional Surveys (SEAC^{4}RS) aircraft campaign, and the contribution of OA to submicron PM was estimated to be ~84% (Liu et al., 2016). Similar results were observed for wildfire emissions, e.g., as can be seen from the aircraft-based South American Biomass Burning Analysis (SAMBBA; Hodgson et al., 2018) project and the Western Wildfire Experiment for Cloud Chemistry, Aerosol Absorption, and Nitrogen (WE-CAN) study (Garofalo et al., 2019).

Although the underprediction of OC by the revised CMAQ could be attributed to the underestimation of open burning emissions by the FINN inventory, this does not necessarily mean that all the ΔOC was caused by the missed primary OC (POC), i.e., missing of secondary OC (SOC) formed from agricultural fire emissions could also be partially responsible. However, based on the available results, ΔOC could not be further separated into POC and SOC. Previous studies focusing on atmospheric aging/transformation of open burning emissions usually showed little or no change of net OA mass (after accounting for dilution) during transport but an increase of the oxygen-to-carbon ratio of OA (Cubison et al., 2011; Jolleys et al., 2012; Hodshire et al., 2019), suggesting aging process and/or SOC formation in plume. However, it remains unclear whether these findings are valid for the agricultural fires impacting HC, given that the distinct environment during HC's open burning period (e.g., the low temperature and the snow over the land) was rarely, if not never, seen in the existing literature.

3.3. Open-burning independent overprediction of EC by the model

The observed EC (EC_{obs}) was typically lower than that simulated by the revised CMAQ (EC_{mod}), frequently resulting in a negative value for their difference ($EC_{obs} - EC_{mod}$, i.e., ΔEC). It appears that the model tended to overpredict EC despite the underestimation of open burning emissions. The comparison of ΔEC and levoglucosan was expected to provide insights into the importance of open burning as an EC source. For example, with the increase of levoglucosan, if the overprediction of EC is observed to be partially or even fully offset, i.e., the negative ΔEC exhibited an increasing trend towards zero, open burning could then be considered as a non-negligible contributor to EC. However, this is not the case for this study. As shown in Fig. 4a, ΔEC was almost independent of levoglucosan, indicating that open burning was not a major source of EC during the measurement period. This inference was consistent with the source apportionment results from Cheng et al. (2021), which were based on the same campaign as this study. Using EPA's Positive Matrix factorization (PMF) model (version 5.0), the authors found that the biomass burning contributions to EC were comparable among various cases with different extents of open burning impact. Given that the different variation patterns of ΔOC and ΔEC with increasing levoglucosan were mainly related to open burning, the biomass burning plumes reaching HC should be characterized by a high OC to EC ratio. This inference was also supported by the relatively low combustion efficiencies suggested for the agricultural fires impacting HC, e.g., the observed chemical signatures such as the EC vs. CO dependence were found to become more characteristic of smoldering combustion with stronger impact of open burning (Cheng et al., 2021).

To identify potential sources responsible for the overprediction of EC by the model, ΔEC was compared with SO_2 and NO_2 obtained from a nearby CNEMC (China National Environmental Monitoring Center) monitoring site. No apparent dependence of ΔEC on SO_2 was indicated (Figure S4), whereas more negative ΔEC values, i.e., more significant overpredictions of EC by the model, were typically associated with relatively high NO_2 concentrations (Fig. 4b). For example, the largest difference between EC_{obs} and EC_{mod} (with a ΔEC of about −21 μg/m^3) was observed at the highest NO_2 concentration (~87 μg/m^3). As indicated by the MEIC inventory (Zheng et al., 2018), both NO_2 and SO_2 have a common source of coal combustion whereas NO_2 itself has vehicle exhausts as a major contributor. Therefore, a likely cause for the overprediction of EC by

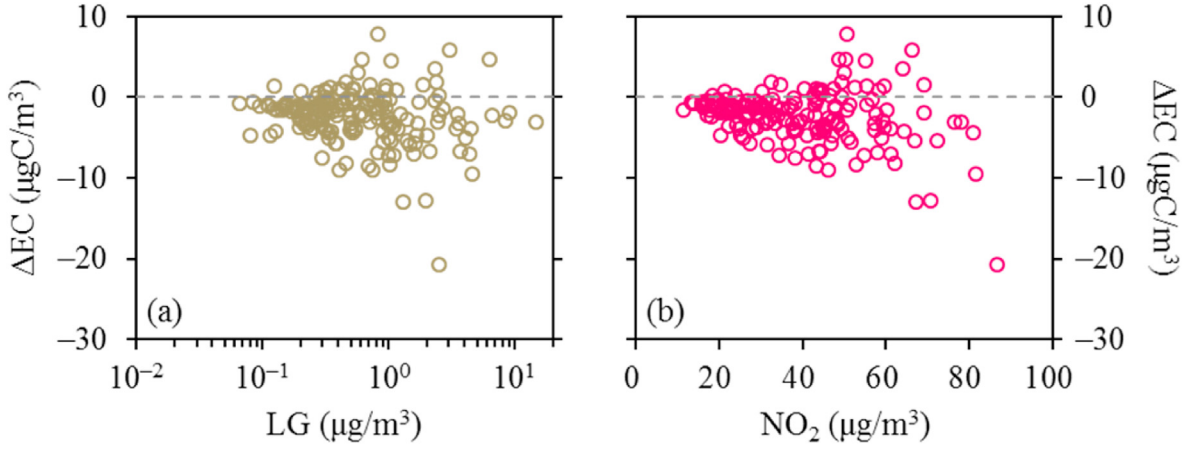

Fig. 4. Dependences of the difference between observed and modeled EC concentrations ($EC_{obs} - EC_{mod}$, i.e., ΔEC) on **(a)** levoglucosan and **(b)** NO_2. The dashed lines indicate a ΔEC value of zero. ΔEC appears independent of levoglucosan whereas significant overestimation of EC by the model (as indicated by a more negative ΔEC) typically occurs at relatively high NO_2.

the revised CMAQ was the overestimation of vehicle emissions by the inventory.

Recalling that the biomass burning contribution to EC (f_{BB}) estimated by the measurement-based PMF analysis was almost independent of open burning (Cheng et al., 2021), it should be acceptable to attribute this f_{BB} to domestic use of biomass fuels (BB_{dom}). The contribution of BB_{dom} to EC could also be derived from the MEIC inventory, which was found to be ~30% in 2017 for the two provinces (i.e., Heilongjiang and Jilin) where HC is located at (Zheng et al., 2018). The inventory-based f_{BB} was lower than the PMF-based estimation (~40%). This pattern was consistent with the inference that EC emissions were likely overestimated for vehicle exhausts (i.e., the transportation sector). It should also be noted that the inventory-based f_{BB} was in terms of annual average, whereas the PMF-based f_{BB} was for the heating season when biomass fuels are expected to be more intensively consumed for heating. Thus, seasonal variation of household biomass use could also be partially responsible for the relatively low inventory-based f_{BB}.

3.4. Model vs. observation discrepancy in nitrate and the role of open burning

Discrepancies were also identified between the measured and simulated nitrate, with their difference ($nitrate_{obs}$ – $nitrate_{mod}$, i.e., Δnitrate) being negative for the majority (57%) of the samples. This indicated that the revised CMAQ frequently overpredicted nitrate, which was likely associated with the overestimation of vehicle emissions (as discussed in the previous section). In addition, as levoglucosan became higher, an increasing trend was observed for Δnitrate (Fig. 5a). More than 70% of the negative Δnitrate values fell into the levoglucosan range of below 0.5 μg/m^3, and the median Δnitrate were approximately −3 μg/m^3 for the two levoglucosan bins corresponding to this range. An increase of Δnitrate was evident at higher levoglucosan, with median values of ~0.3, 1.7 and 3.7 μg/m^3 for the levoglucosan ranges of 0.5–1, 1–2 and above 2 μg/m^3, respectively (refer to Figure S5a for the detailed box plot). The positive dependence of Δnitrate on levoglucosan indicated that the underestimation of open burning would result in an underprediction of nitrate by the model, and with stronger open burning influence, this underprediction would offset and finally overwhelm the opposite effect caused by the overestimation of vehicle emissions. In other words, the positive dependence of Δnitrate on levoglucosan pointed to a considerable influence of open burning on nitrate. Given that nitrate is commonly considered secondary and biomass burning is typically not an important source of nitrogen oxides (NO_x; Zheng et al., 2018), it was inferred that the oxidation of NO_x was likely enhanced when impacted by open burning, which can be a significant source of hydrogen oxide radicals (HO_x; e.g., Akagi et al., 2012) and organic peroxy radicals (RO_2; e.g., Orlando and Tyndall, 2012).

It was noticed that the largest Δnitrate (~20 μg/m^3) was observed at a levoglucosan of 4.60 μg/m^3 rather than at its highest concentration. This sample corresponded to the Lantern Festival and exhibited the highest K^+ during the campaign. In addition to open burning, therefore, it should also be significantly impacted by firework emissions (Cheng et al., 2021) which were not involved in the MEIC inventory. Consequently, the large Δnitrate observed for this sample should be attributed to not only the underprediction of open-burning related nitrate but also the missing of that associated with fireworks.

3.5. Model vs. observation discrepancy in sulfate

The difference in the observed and modeled sulfate ($sulfate_{obs}$ – $sulfate_{mod}$, i.e., Δsulfate) exhibited a positive dependence on levoglucosan as well. However, the largest Δsulfate values (~15–23 μg/m^3) were not observed at the highest levoglucosan (Fig. 5b). Instead, they occurred for three distinct sampling events in January, which were characterized by enhanced sulfate formation at high RH levels (above ~80%; Figure S6), presumably through heterogeneous chemistry in aerosol water (Cheng et al., 2020). Although a heterogeneous pathway for the oxidation of SO_2 to sulfate (parameterized by the apparent, i.e., bulk, reactive uptake coefficient of SO_2) had been involved in the revised CAMQ, it seems that the model still could not properly reproduce the observed sulfate (with substantial underestimations) when heterogeneous chemistry was evident. Unlike this study, however, the same model was found to significantly overestimate sulfate concentrations for high RH conditions during winter in Beijing (Liu et al., 2020). The conflicted results indicated that the model needs to be further

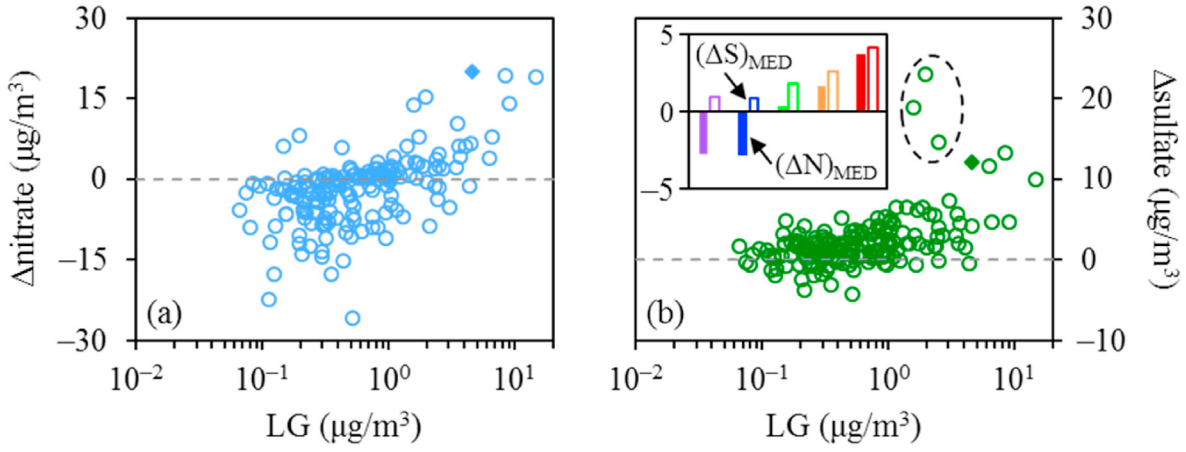

Fig. 5. Dependences of **(a)** the difference between observed and modeled nitrate concentrations ($nitrate_{obs}$ – $nitrate_{mod}$, i.e., Δnitrate) and **(b)** the difference between observed and modeled sulfate concentrations ($sulfate_{obs}$ – $sulfate_{mod}$, i.e., Δsulfate) on levoglucosan. The dashed lines indicate a Δnitrate or Δsulfate value of zero, while a sample heavily impacted by firework emissions is highlighted by the solid diamonds. In (b), three samples showing clear evidence for heterogeneous sulfate formation are highlighted by the dashed oval. They were not involved when comparing the median Δsulfate (in μg/m^3), i.e., $(\Delta S)_{MED}$, across different levoglucosan ranges, as shown by the open bars in the inner chart. The levoglucosan bins are below 0.2 (purple), 0.2–0.5 (blue), 0.5–1 (green), 1–2 (orange) and above 2 μg/m^3 (red). The median Δnitrate results (in μg/m^3), i.e., $(\Delta N)_{MED}$, are also presented (by the solid bars) in the inner chart for comparison. (For interpretation of the references to color in this figure legend, the reader is referred to the Web version of this article.)

improved, e.g., by adding detailed heterogeneous reactions.

After excluding the three distinct samples, the dependence of Δsulfate on levoglucosan exhibited a more consistent increasing trend (Fig. 5b and S5b). As discussed for nitrate, this positive dependence pointed to the influence of open burning on sulfate formation. However, with increasing levoglucosan, the increase of Δsulfate was less sharp than Δnitrate, and relatively large Δsulfate (~10 μg/m^3) were evident only at the higher end of the levoglucosan concentrations (Fig. 5b). Therefore, nitrate formation was more strongly impacted by open burning. This is not surprising, given the relatively slow gas-phase oxidation of SO_2 (Akagi et al., 2012).

4. Conclusions

Field observation and a revised CMAQ model were combined to investigate the $PM_{2.5}$ pollution during heating season in Harbin. Significant underprediction of $PM_{2.5}$ concentration was identified at elevated levoglucosan (above 0.5 μg/m^3), likely due to the underestimation of open burning emissions by the model. With evident influence of open burning, the revised CMAQ considerably underpredicted OC as well, and ΔOC was usually found to be the dominant driver of $\Delta PM_{2.5}$. However, despite the underestimation of open burning, the model tended to overpredict EC. Given that ΔEC was independent of levoglucosan but became more negative with increasing NO_2, vehicle emissions were likely overestimated by the model. This inference also explained the negative Δnitrate at low levoglucosan. With increasing levoglucosan, however, Δnitrate increased towards zero and finally became positive, pointing to the enhancement of nitrate formation by open burning. Influence of open burning on sulfate formation was apparent only at the higher end of levoglucosan concentrations. In addition, the model failed to reproduce the observed sulfate (with large underestimations) when heterogeneous chemistry was evident.

This study demonstrates that uncertainties in open burning emissions could introduce substantial difficulties to $PM_{2.5}$ simulation, for not only primary components but also secondary species. In addition, similar to previous work in NCP, this study suggests that the CMAQ model needs to be improved for the simulation of secondary aerosol formed through heterogeneous chemistry.

Credit author statement

Yuan Cheng: Conceptualization, Methodology, Writing-Original Draft. Jiu-meng Liu: Conceptualization, Methodology, Writing-Review & Editing. Qin-qin Yu, Shengqiang Zhu and Mengyuan Zhang: Investigation. Hong-liang Zhang and Bo Zheng: Methodology, Validation. Ke-bin He: Supervision.

Declaration of competing interest

The authors declare that they have no known competing financial interests or personal relationships that could have appeared to influence the work reported in this paper.

Acknowledgments

This work was supported by the National Natural Science Foundation of China (41805097, 4151101089), the Natural Science Foundation of Heilongjiang Province (YQ2019D004), the National Key Research and Development Program (2019YFC0214700), the State Key Laboratory of Urban Water Resource and Environment (2020DX14), the State Key Joint Laboratory of Environment Simulation and Pollution Control (19K02ESPCT), the State Environmental Protection Key Laboratory of Sources and Control of Air Pollution Complex (SCAPC202002) and the Key Laboratory of Atmospheric Chemistry, China Meteorological Administration (2019B04).

Appendix A. Supplementary data

Supplementary data to this article can be found online at https://doi.org/10.1016/j.envpol.2020.116167.

References

Akagi, S.K., Craven, J.S., Taylor, J.W., McMeeking, G.R., Yokelson, R.J., Burling, I.R., Urbanski, S.P., Wold, C.E., Seinfeld, J.H., Coe, H., Alvarado, M.J., Weise, D.R., 2012. Evolution of trace gases and particles emitted by a chaparral fire in California. Atmos. Chem. Phys. 12, 1397–1421.

Cai, S.Y., Wang, Y.J., Zhao, B., Wang, S.X., Chang, X., Hao, J.M., 2017. The impact of the "air pollution prevention and control action plan" on $PM_{2.5}$ concentrations in Jing-Jin-Ji region during 2012–2020. Sci. Total Environ. 580, 197–209.

Cheng, Y., Engling, G., He, K.B., Duan, F.K., Ma, Y.L., Du, Z.Y., Liu, J.M., Zheng, M., Weber, R.J., 2013. Biomass burning contribution to Beijing aerosol. Atmos. Chem. Phys. 13, 7765–7781.

Cheng, Y., Yu, Q.Q., Liu, J.M., Du, Z.Y., Liang, L.L., Geng, G.N., Ma, W.L., Qi, H., Zhang, Q., He, K.B., 2020. Secondary inorganic aerosol during heating season in a megacity in Northeast China: evidence for heterogeneous chemistry in severe cold climate region. Chemosphere 261, 127769.

Cheng, Y., Yu, Q.Q., Liu, J.M., Du, Z.Y., Liang, L.L., Geng, G.N., Zheng, B., Ma, W.L., Qi, H., Zhang, Q., He, K.B., 2021. Strong biomass burning contribution to ambient aerosol during heating season in a megacity in Northeast China: effectiveness of agricultural fire bans? Sci. Total Environ. 754, 142144.

Cheng, Y.F., Zheng, G.J., Wei, C., Mu, Q., Zheng, B., Wang, Z.B., Gao, M., Zhang, Q., He, K.B., Carmichael, G., Pöschl, U., Su, H., 2016. Reactive nitrogen chemistry in aerosol water as a source of sulfate during haze events in China. Sci. Adv. 2, e1601530 https://doi.org/10.1126/sciadv.1601530.

Cheng, Z., Wang, S., Fu, X., Watson, J.G., Jiang, J., Fu, Q., Chen, C., Xu, B., Yu, J., Chow, J.C., Hao, J., 2014. Impact of biomass burning on haze pollution in the Yangtze River delta, China: a case study in summer 2011. Atmos. Chem. Phys. 14, 4573–4585.

Chu, B.W., Ma, Q.X., Duan, F.K., Ma, J.Z., Jiang, J.K., He, K.B., He, H., 2020. Atmospheric "haze chemistry": concept and research prospects. Prog. Chem. 32, 1–4.

Cubison, M.J., Ortega, A.M., Hayes, P.L., Farmer, D.K., Day, D., Lechner, M.J., Brune, W.H., Apel, E., Diskin, G.S., Fisher, J.A., Fuelberg, H.E., Hecobian, A., Knapp, D.J., Mikoviny, T., Riemer, D., Sachse, G.W., Sessions, W., Weber, R.J., Weinheimer, A.J., Wisthaler, A., Jimenez, J.L., 2011. Effects of aging on organic aerosol from open biomass burning smoke in aircraft and laboratory studies. Atmos. Chem. Phys. 11, 12049–12064.

Dao, X., Lin, Y.C., Cao, F., Di, S.Y., Hong, Y.H., Xing, G.H., Li, J.J., Fu, P.Q., Zhang, Y.L., 2019. Introduction to the national aerosol chemical composition monitoring network of China: objectives, current status, and outlook. Bull. Am. Meteorol. Soc. 100, ES337–ES351.

Department of Ecology and Environment of Heilongjiang Province, 2018. Interim provisions of Heilongjiang province on reward and punishment for straw open burning management. Available at: http://sthj.hlj.gov.cn/tzgg/2018/09/20510.html.

Garofalo, L.A., Pothier, M.A., Levin, E.J.T., Campos, T., Kreidenweis, S.M., Farmer, D.K., 2019. Emission and evolution of submicron organic aerosol in smoke from wildfires in the Western United States. ACS Earth Space Chem. 3, 1237–1247.

Gu, Y.F., Huang, R.J., Li, Y.J., Duan, J., Chen, Q., Hu, W.W., Zheng, Y., Lin, C.S., Ni, H.Y., Dai, W.T., Cao, J.J., Liu, Q., Chen, Y., Chen, C.Y., Ovadnevaite, J., Ceburnis, D., O'Dowd, C., 2020. Chemical nature and sources of fine particles in urban Beijing: seasonality and formation mechanisms. Environ. Int. 140, 105732.

Hodgson, A.K., Morgan, W.T., O'Shea, S., Bauguitte, S., Allan, J.D., Darbyshire, E., Flynn, M.J., Liu, D.T., Lee, J., Johnson, B., Haywood, J.M., Longo, K.M., Artaxo, P.E., Coe, H., 2018. Near-field emission profiling of tropical forest and Cerrado fires in Brazil during SAMBBA 2012. Atmos. Chem. Phys. 18, 5619–5638.

Hodshire, A.L., Akherati, A., Alvarado, M.J., Brown-Steiner, B., Jathar, S.H., Jimenez, J.L., Kreidenweis, S.M., Lonsdale, C.R., Onasch, T.B., Ortega, A.M., Pierce, J.R., 2019. Aging effects on biomass burning aerosol mass and composition: a critical review of field and laboratory studies. Environ. Sci. Technol. 53, 10007–10022.

Hu, J.L., Chen, J.J., Ying, Q., Zhang, H.L., 2016a. One-year simulation of ozone and particulate matter in China using WRF/CMAQ modeling system. Atmos. Chem. Phys. 16, 10333–10350.

Hu, W.W., Hu, M., Hu, W., Jimenez, J.L., Yuan, B., Chen, W.T., Wang, M., Wu, Y.S., Chen, C., Wang, Z.B., Peng, J.F., Zeng, L.M., Shao, M., 2016b. Chemical composition, sources, and aging process of submicron aerosols in Beijing: contrast between summer and winter. J. Geophys. Res. Atmos. 121, 1955–1977.

Jolleys, M.D., Coe, H., McFiggans, G., Capes, G., Allan, J.D., Crosier, J., Williams, P.I., Allen, G., Bower, K.N., Jimenez, J.L., Russell, L.M., Grutter, M., Baumgardner, D., 2012. Characterizing the aging of biomass burning organic aerosol by use of mixing ratios: a meta-analysis of four regions. Environ. Sci. Technol. 46, 13093–13102.

Konovalov, I.B., Lvova, D.A., Beekmann, M., Jethva, H., Mikhailov, E.F., Paris, J.D., Belan, B.D., Kozlov, V.S., Ciais, P., Andreae, M.O., 2018. Estimation of black carbon

emissions from Siberian fires using satellite observations of absorption and extinction optical depths. Atmos. Chem. Phys. 18, 14889–14924.
Lasko, K., Vadrevu, K.P., Tran, V.T., Ellicott, E., Nguyen, T.T.N., Bui, H.Q., Justice, C., 2017. Satellites may underestimate rice residue and associated burning emissions in Vietnam. Environ. Res. Lett. 12, 085006.
Li, H.Y., Cheng, J., Zhang, Q., Zheng, B., Zhang, Y.X., Zheng, G.J., He, K.B., 2019a. Rapid transition in winter aerosol composition in Beijing from 2014 to 2017: response to clean air actions. Atmos. Chem. Phys. 19, 11485–11499.
Li, K., Jacob, D.J., Liao, H., Shen, L., Zhang, Q., Bates, K.H., 2019b. Anthropogenic drivers of 2013–2017 trends in summer surface ozone in China. Proc. Natl. Acad. Sci. U. S. A 116, 422–427.
Liu, J.M., Wang, P.F., Zhang, H.L., Du, Z.Y., Zheng, B., Yu, Q.Q., Zheng, G.J., Ma, Y.L., Zheng, M., Cheng, Y., Zhang, Q., He, K.B., 2020. Integration of field observation and air quality modeling to characterize Beijing aerosol in different seasons. Chemosphere 242, 125195.
Liu, X.X., Zhang, Y., Huey, L.G., Yokelson, R.J., Wang, Y., Jimenez, J.L., Campuzano-Jost, P., Beyersdorf, A.J., Blake, D.R., Choi, Y., St Clair, J.M., Crounse, J.D., Day, D.A., Diskin, G.S., Fried, A., Hall, S.R., Hanisco, T.F., King, L.E., Meinardi, S., Mikoviny, T., Palm, B.B., Peischl, J., Perring, A.E., Pollack, I.B., Ryerson, T.B., Sachse, G., Schwarz, J.P., Simpson, I.J., Tanner, D.J., Thornhill, K.L., Ullmann, K., Weber, R.J., Wennberg, P.O., Wisthaler, A., Wolfe, G.M., Ziemba, L.D., 2016. Agricultural fires in the southeastern U.S. during SEAC^{4}RS: emissions of trace gases and particles and evolution of ozone, reactive nitrogen, and organic aerosol. J. Geophys. Res. Atmos. 121, 7383–7414.
Ming, L.L., Jin, L., Li, J., Fu, P.Q., Yang, W.Y., Liu, D., Zhang, G., Wang, Z.F., Li, X.D., 2017. $PM_{2.5}$ in the Yangtze River Delta, China: chemical compositions, seasonal variations, and regional pollution events. Environ. Pollut. 223, 200–212.
Orlando, J.J., Tyndall, G.S., 2012. Laboratory studies of organic peroxy radical chemistry: an overview with emphasis on recent issues of atmospheric significance. Chem. Soc. Rev. 41, 6294–6317.
Pan, X.H., Ichoku, C., Chin, M., Bian, H.S., Darmenov, A., Colarco, P., Ellison, L., Kucsera, T., da Silva, A., Wang, J., Oda, T., Cui, G., 2020. Six global biomass burning emission datasets: intercomparison and application in one global aerosol model. Atmos. Chem. Phys. 20, 969–994.
Qiu, X.H., Duan, L., Chai, F.H., Wang, S.X., Yu, Q., Wang, S.L., 2016. Deriving high-resolution emission inventory of open biomass burning in China based on satellite observations. Environ. Sci. Technol. 50, 11779–11786.
Reddington, C.L., Morgan, W.T., Darbyshire, E., Brito, J., Coe, H., Artaxo, P., Scott, C.E., Marsham, J., Spracklen, D.V., 2019. Biomass burning aerosol over the Amazon: analysis of aircraft, surface and satellite observations using a global aerosol model. Atmos. Chem. Phys. 19, 9125–9152.
Reddington, C.L., Spracklen, D.V., Artaxo, P., Ridley, D.A., Rizzo, L.V., Arana, A., 2016. Analysis of particulate emissions from tropical biomass burning using a global aerosol model and long-term surface observations. Atmos. Chem. Phys. 16, 11083–11106.
Samset, B.H., Myhre, G., Herber, A., Kondo, Y., Li, S.M., Moteki, N., Koike, M., Oshima, N., Schwarz, J.P., Balkanski, Y., Bauer, S.E., Bellouin, N., Berntsen, T.K., Bian, H., Chin, M., Diehl, T., Easter, R.C., Ghan, S.J., Iversen, T., Kirkevåg, A., Lamarque, J.F., Lin, G., Liu, X., Penner, J.E., Schulz, M., Seland, Ø., Skeie, R.B., Stier, P., Takemura, T., Tsigaridis, K., Zhang, K., 2014. Modelled black carbon radiative forcing and atmospheric lifetime in AeroCom Phase II constrained by aircraft observations. Atmos. Chem. Phys. 14, 12465–12477.
Sun, Y.L., Du, W., Fu, P.Q., Wang, Q.Q., Li, J., Ge, X.L., Zhang, Q., Zhu, C.M., Ren, L.J., Xu, W.Q., Zhao, J., Han, T.T., Worsnop, D.R., Wang, Z.F., 2016a. Primary and secondary aerosols in Beijing in winter: sources, variations and processes. Atmos. Chem. Phys. 16, 8309–8329.
Sun, Y.L., Jiang, Q., Xu, Y.S., Ma, Y., Zhang, Y.J., Liu, X.G., Li, W.J., Wang, F., Li, J., Wang, P.C., Li, Z.Q., 2016b. Aerosol characterization over the North China Plain: haze life cycle and biomass burning impacts in summer. J. Geophys. Res. Atmos. 121, 2508–2521.
Sun, Y.L., Xu, W.Q., Zhang, Q., Jiang, Q., Canonaco, F., Prévôt, A.S.H., Fu, P.Q., Li, J., Jayne, J., Worsnop, D.R., Wang, Z.F., 2018. Source apportionment of organic aerosol from 2-year highly time-resolved measurements by an aerosol chemical speciation monitor in Beijing, China. Atmos. Chem. Phys. 18, 8469–8489.
Uranishi, K., Ikemori, F., Shimadera, H., Kondo, A., Sugata, S., 2019. Impact of field biomass burning on local pollution and long-range transport of $PM_{2.5}$ in Northeast Asia. Environ. Pollut. 244, 414–422.
Wang, Q.L., Wang, L.L., Li, X.R., Xin, J.Y., Liu, Z.R., Sun, Y., Liu, J.D., Zhang, Y.J., Du, W., Jin, X., Zhang, T.R., Liu, S.Q., Liu, Q., Chen, J., Cheng, M.M., Wang, Y.S., 2020. Emission characteristics of size distribution, chemical composition and light absorption of particles from field-scale crop residue burning in Northeast China. Sci. Total Environ. 710, 136304.
Wang, Y.X., Zhang, Q.Q., Jiang, J.K., Zhou, W., Wang, B.Y., He, K.B., Duan, F.K., Zhang, Q., Philip, S., Xie, Y.Y., 2014. Enhanced sulfate formation during China's severe winter haze episode in January 2013 missing from current models. J. Geophys. Res. Atmos. 119, 10425–10440.
Wei, J., Li, Z.Q., Guo, J.P., Sun, L., Huang, W., Xue, W.H., Fan, T.Y., Cribb, M., 2019. Satellite-derived 1-km-resolution PM_1 concentrations from 2014 to 2018 across China. Environ. Sci. Technol. 53, 13265–13274.
Wiedinmyer, C., Akagi, S.K., Yokelson, R.J., Emmons, L.K., Al-Saadi, J.A., Orlando, J.J., Soja, A.J., 2011. The Fire INventory from NCAR (FINN): a high resolution global model to estimate the emissions from open burning. Geosci. Model Dev. 4, 625–641.
Xu, W.Q., Sun, Y.L., Wang, Q.Q., Zhao, J., Wang, J.F., Ge, X.L., Xie, C.H., Zhou, W., Du, W., Li, J., Fu, P.Q., Wang, Z.F., Worsnop, D.R., Coe, H., 2019. Changes in aerosol chemistry from 2014 to 2016 in winter in Beijing: insights from high-resolution aerosol mass spectrometry. J. Geophys. Res. Atmos. 124, 1132–1147.
Yan, C.Q., Sullivan, A.P., Cheng, Y., Zheng, M., Zhang, Y.H., Zhu, T., Collett Jr., J.L., 2019. Characterization of saccharides and associated usage in determining biogenic and biomass burning aerosols in atmospheric fine particulate matter in the North China Plain. Sci. Total Environ. 650, 2939–2950.
Zhai, S.X., Jacob, D.J., Wang, X., Shen, L., Li, K., Zhang, Y.Z., Gui, K., Zhao, T.L., Liao, H., 2019. Fine particulate matter ($PM_{2.5}$) trends in China, 2013–2018: separating contributions from anthropogenic emissions and meteorology. Atmos. Chem. Phys. 19, 11031–11041.
Zhang, Q., Zheng, Y.X., Tong, D., Shao, M., Wang, S.X., Zhang, Y.H., Xu, X.D., Wang, J.N., He, H., Liu, W.Q., Ding, Y.H., Lei, Y., Li, J.H., Wang, Z.F., Zhang, X.Y., Wang, Y.S., Cheng, J., Liu, Y., Shi, Q.R., Yan, L., Geng, G.N., Hong, C.P., Li, M., Liu, F., Zheng, B., Cao, J.J., Ding, A.J., Gao, J., Fu, Q.Y., Huo, J.T., Liu, B.X., Liu, Z.R., Yang, F.M., He, K.B., Hao, J.M., 2019. Drivers of improved $PM_{2.5}$ air quality in China from 2013 to 2017. Proc. Natl. Acad. Sci. U. S. A 116, 24463–24469.
Zheng, B., Tong, D., Li, M., Liu, F., Hong, C.P., Geng, G.N., Li, H.Y., Li, X., Peng, L.Q., Qi, J., Yan, L., Zhang, Y.X., Zhao, H.Y., Zheng, Y.X., He, K.B., Zhang, Q., 2018. Trends in China's anthropogenic emissions since 2010 as the consequence of clean air actions. Atmos. Chem. Phys. 18, 14095–14111.
Zheng, B., Zhang, Q., Zhang, Y., He, K.B., Wang, K., Zheng, G.J., Duan, F.K., Ma, Y.L., Kimoto, T., 2015. Heterogeneous chemistry: a mechanism missing in current models to explain secondary inorganic aerosol formation during the January 2013 haze episode in North China. Atmos. Chem. Phys. 15, 2031–2049.
Zhou, Y., Xing, X.F., Lang, J.L., Chen, D.S., Cheng, S.Y., Wei, L., Wei, X., Liu, C., 2017. A comprehensive biomass burning emission inventory with high spatial and temporal resolution in China. Atmos. Chem. Phys. 17, 2839–2864.